J Occup Health 2018; 60: 148-155

Journal of Occupational Health

Original

Nitrative DNA damage in cultured macrophages exposed to indium oxide

Tahmina Afroz[1], Yusuke Hiraku[1], Ning Ma[2], Sharif Ahmed[1], Shinji Oikawa[1], Shosuke Kawanishi[3] and Mariko Murata[1]

[1]Department of Environmental and Molecular Medicine, Mie University Graduate School of Medicine, Mie, Japan, [2]Faculty of Nursing, Suzuka University of Medical Science, Mie, Japan and [3]Faculty of Pharmaceutical Sciences, Suzuka University of Medical Science, Mie, Japan

Abstract: Objectives: Indium compounds are used in manufacturing displays of mobile phones and televisions. However, these materials cause interstitial pneumonia in exposed workers. Animal experiments demonstrated that indium compounds caused lung cancer. Chronic inflammation is considered to play a role in lung carcinogenesis and fibrosis induced by particulate matters. 8-Nitroguanine (8-nitroG) is a mutagenic DNA lesion formed during inflammation and may participate in carcinogenesis. To clarify the mechanism of carcinogenesis, we examined 8-nitroG formation in indium-exposed cultured cells. **Methods:** We treated RAW 264.7 mouse macrophages with indium oxide (In_2O_3) nanoparticles (primary diameter: 30-50 nm), and performed fluorescent immunocytochemistry to detect 8-nitroG. The extent of 8-nitroG formation was evaluated by quantitative image analysis. We measured the amount of nitric oxide (NO) in the culture supernatant of In_2O_3-treated cells by the Griess method. We also examined the effects of inhibitors of inducible NO synthase (iNOS) and endocytosis on In_2O_3-induced 8-nitroG formation. **Results:** In_2O_3 significantly increased the intensity of 8-nitroG formation in RAW 264.7 cells in a dose-dependent manner. In_2O_3-induced 8-nitroG formation was observed at 2 h and further increased at 4 h, and the amount of NO released from In_2O_3-exposed cells was significantly increased at 2-4 h compared with the control. 8-NitroG formation was suppressed by 1400W (an iNOS inhibitor), methyl-β-cyclodextrin and monodansylcadaverine (inhibitors of caveolae- and clathrin-mediated endocytosis, respectively). **Conclusions:** These results suggest that endocytosis and NO generation participate in indium-induced 8-nitroG formation. NO released from indium-exposed inflammatory cells may induce DNA damage in adjacent lung epithelial cells and contribute to carcinogenesis.
(J Occup Health 2018; 60: 148-155)
doi: 10.1539/joh.17-0146-OA

Key words: 8-Nitroguanine, DNA damage, Endocytosis, Indium, Inflammation, Nitric oxide

Introduction

Indium has been used as a metal, in alloys, and for electronics application. The worldwide demand for indium metal has increased noticeably in recent years due to growth of microelectronics industry. Indium compounds, especially indium-tin oxide (ITO), have been used for the production of liquid crystal displays, mobile phone displays and solar cells due to their characteristics of high electrical conductivity, transparency and mechanical resistance. The first case of indium-related interstitial pneumonia in a worker who had been working as a grinder in an ITO target manufacturing facility in Japan was reported in 2003[1)]. An epidemiological study has demonstrated the relationship between indium exposure and interstitial changes in the lungs detected by high-resolution computed tomography[2)]. A similar causal relationship between indium exposure and interstitial lung disorders has been reported in Korea[3)]. In addition, two cases of pulmonary alveolar proteinosis in the United States and one case of pulmonary alveolar proteinosis in

Received June 8, 2017; Accepted November 8, 2017
Published online in J-STAGE November 29, 2017
Correspondence to: Y. Hiraku, Department of Environmental and Molecular Medicine, Mie University Graduate School of Medicine, Tsu, Mie 514-8507, Japan (e-mail: y-hiraku@doc.medic.mie-u.ac.jp)
Supplementary materials (Appendices) are available in the online version of this article

China have been reported[4,5]. A recent 5-year follow-up study was conducted on indium-exposed workers and long-term adverse effects on emphysematous changes were observed[6]. Lung carcinogenicity has been observed in long-term inhalation studies with indium compounds in experimental animals. A 2-year animal experiment of ITO inhalation revealed that there was a clear evidence of lung carcinogenicity in male and female rats[7]. Recently, ITO has been evaluated as a Group 2B carcinogen (possibly carcinogenic to humans) by the International Agency for Research on Cancer (IARC)[8,9]. In addition, indium phosphide has been classified as a Group 2A carcinogen (probably carcinogenic to human) by IARC[10]. These findings raise a concern that lung cancer may occur in humans exposed to indium compounds in the future.

Inhalation exposure to particulate matters causes chronic inflammation in the respiratory systems, leading to lung carcinogenesis and fibrosis. Chronic inflammation, which is induced by various environmental factors such as infection, inflammatory diseases and physicochemical agents, is postulated to play a substantial part in human carcinogenesis[11,12]. Under inflammatory conditions, reactive oxygen species (ROS) and reactive nitrogen species (RNS) are generated in inflammatory and epithelial cells. These reactive species interact with DNA bases to form oxidative and nitrative DNA lesions[13,14]. 8-Nitroguanine (8-nitroG) is a mutagenic nitrative DNA lesion formed during chronic inflammation. Nitric oxide (NO) reacts with superoxide ($O_2^{\cdot -}$) to form highly reactive peroxide ($ONOO^-$), which interacts with guanine to form 8-nitroG[15]. 8-NitroG was formed at the sites of carcinogenesis in various animal models and clinical specimens of cancer-prone inflammatory diseases and is expected to be a potential biomarker of inflammation-related carcinogenesis[16,17]. We have demonstrated that 8-nitroG was formed in cultured macrophage and lung epithelial cells by particulate matters, including multiwalled carbon nanotube[18,19] and carbon black[20].

In this study, to investigate the mechanism of indium-induced genotoxicity and carcinogenicity, we performed immunocytochemical analysis to examine 8-nitroG formation in RAW 264.7 mouse macrophages treated with indium oxide (In_2O_3), which accounts for a large part (approximately 90%-95%) of ITO. We used RAW 264.7 cells in this study, because macrophages in airway and alveolar spaces play a substantial role in lung carcinogenesis via the interaction with epithelial cells[21,22]. Macrophages initially contact and engulf inhaled particles, and then release ROS, RNS and inflammatory cytokines. These molecules secondarily induce the generation of reactive species and the expression of inflammatory molecules in adjacent epithelial cells, leading to lung carcinogenesis[21]. We have previously reported that endocytosis plays a role in DNA damage caused by particulate matters[18-20]. To clarify the mechanism of indium-induced genotoxicity, we examined the effects of endocytosis inhibitors on 8-nitroG formation.

Materials and Methods

Preparation of In_2O_3 particles

In_2O_3 nanoparticles (primary diameter: 30-50 nm) were obtained from Nanostructured and Amorphous Materials, Inc. (Houston, TX, USA). Purity was 99.99% and surface area was 15 m^2/g (disclosed by the manufacturer). In_2O_3 was suspended in Dulbecco's Modified Eagles Medium (DMEM, Gibco/BRL, New York, NY, USA) containing 5% (v/v) heat-inactivated fetal bovine serum (FBS) and 100 mg/*l* kanamycin. The suspension was vortexed for 1 min and then sonicated for 20 min at 40 W with an ultrasonic homogenizer (Model 450 Branson Ultrasonic, Danbury, CT, USA) to disperse agglomerates as described previously[19]. The suspensions of the agglomerates were stored at −80°C until use. We thawed and vortexed the suspensions to use for experiments, and measured the size distributions of the agglomerates with a Zetasizer Nano particle size analyzer (Malvern, Worcestershire, UK) as described previously[19,20].

Evaluation of indium-induced cytotoxicity

We evaluated In_2O_3-induced cytotoxicity by trypan blue exclusion assay. RAW 264.7 mouse macrophage cells (5×10^5 cells/m*l*, RIKEN BioResource Center, Tsukuba, Japan) were seeded in 1.2 m*l* of DMEM containing 5% (v/v) FBS and 100 mg/*l* kanamycin in 6 Well Clear Multiwell Plates (BD Falcon, Franklin Lakes, NJ, USA). Immediately after seeding, the cells were incubated with 0-50 μg/m*l* of In_2O_3 for 24 h at 37°C in an atmosphere containing 5% CO_2. We employed these concentrations of In_2O_3, because we have previously demonstrated that other types of nanomaterials induced significant cytotoxic and/or genotoxic effects at similar concentrations[18,20]. Then, the cell suspensions were mixed with trypan blue, and the viability was calculated with a TC20 Automated cell counter (Bio-Rad Laboratories, Hercules CA, USA).

Detection of 8-nitroG formation

Localization of 8-nitroG formation in In_2O_3-exposed cells was assessed by immunocytochemical analysis as described previously[20]. RAW 264.7 cells (5×10^5 cells/m*l*) were seeded in 1.2 m*l* of DMEM containing 5% (v/v) FBS and 100 mg/*l* kanamycin in 6 Well Clear Multiwell Plates (BD Falcon). Then, the cells were incubated with In_2O_3 for 2 or 4 h at 37°C in an atmosphere containing 5% CO_2. In a certain experiment, RAW 264.7 cells were co-treated with 1 μM 1400 W [an inhibitor of inducible NO synthase (iNOS)], 0.5 mM methyl-β-cyclodextrin (MBCD, an inhibitor of caveolae-mediated endocytosis), 50 μM monodansylcadaverine (MDC, an inhibitor of

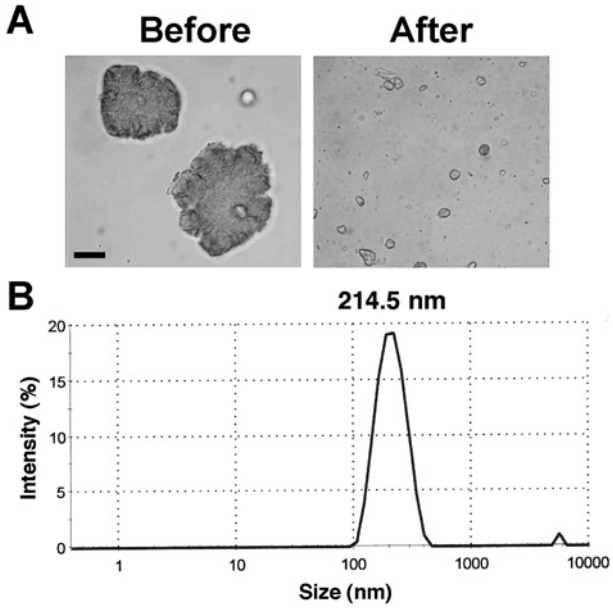

Fig. 1. Dispersion of In_2O_3 agglomerates. In_2O_3 was suspended in DMEM and sonicated as described in Materials and Methods section. (A) In_2O_3 agglomerates before and after the sonication. The agglomerates were observed with a light microscope. Bar = 10 μm. (B) Size distribution of dispersed In_2O_3 particles. The size distribution was measured with a Zetasizer Nano particle size analyzer (Malvern Worcestershire UK).

clathrin-mediated endocytosis). We employed these concentrations of the inhibitors, because they did not show significant cytotoxic effects as described in the Results section. These inhibitors were purchased from Sigma-Aldrich (St. Louis, MO, USA).

After the treatment with In_2O_3, the cells were fixed with 4% (v/v) formaldehyde in phosphate buffered saline (PBS) for 10 min at room temperature and washed with PBS. Then, the cells were treated with 0.5% (v/v) Triton X100 for 3 min and incubated with 1% (w/v) skim milk for 1 h at room temperature. To detect 8-nitroG, the cells were incubated with rabbit polyclonal anti-8-nitroG antibody (1 μg/m*l*) produced by our group[23,24] overnight at room temperature. Then the cells were incubated with fluorescent secondary antibody [Alexa 594-labeled goat antibody against rabbit IgG (1:400, molecular probes, Eugene, OR, USA)] for 3 h. The nuclei were stained with 5 μM Hoechst 33258 (Polysciences Inc., Warrington, PA, USA). The stained cells were examined under florescent microscope (BX53, Olympus, Tokyo, Japan). Staining intensity of 8-nitroG per cell was quantified by analyzing 3-5 randomly selected fields per sample, containing approximately 800 cells in average, with an ImageJ software.

Analysis of NO products

To analyze NO released from In_2O_3-treated cells, we measured the concentration of its products, nitrate (NO_3^-) and nitrite (NO_2^-), in the culture supernatant by using the Griess method. RAW 264.7 cells (5×10^5 cells/m*l*) were seeded in 1.2 m*l* of phenol red-free DMEM (Gibco/BRL) containing 5% (v/v) FBS and 100 mg/*l* kanamycin in 6 Well Clear Multiwell Plates (BD Falcon). Then the cells were treated with 20 μg/m*l* In_2O_3 for 2 or 4 h at 37°C. The culture supernatant was collected and centrifuged at 40,000 × g for 10 min at 4°C to remove In_2O_3 particles. To reduce NO_3^- to NO_2^-, the supernatant was incubated with 0.1 units/m*l* of nitrate reductase from *Aspergillus niger* (Sigma-Aldrich) in the presence of 1 mM glucose-6-phosphate (Wako Pure Chemical Industries, Osaka, Japan), 0.3 units/m*l* of glucose-6-phosphate dehydrogenase and 20 μM NADPH (Oriental Yeast, Tokyo, Japan) for 30 min at room temperature. The reaction mixture was incubated with 0.25% (w/v) sulfanilamide (Griess reagent I, Wako) and 0.025% (w/v) naphthylethylenediamine (Griess reagent II, Sigma-Aldrich) in 0.625% (v/v) phosphoric acid for 10 min at room temperature. The absorbance was measured at 540 nm with a microplate reader (Model 680, Bio-Rad laboratories) and NO_2^- concentration was determined by comparison with a standard curve generated with sodium nitrate ($NaNO_2$, Wako).

Statistical analysis

Statistical analysis was performed by one-way analysis of variance (ANOVA) followed by Tukey's multiple comparison test or Student's *t*-test using an SPSS software (20.0 for Mac). Results were presented as means± SD. Probability values less than 0.05 were considered to be statistically significant.

Results

Dispersion and size distribution of In_2O_3

We suspended In_2O_3 in DMEM and dispersed agglomerates with an ultrasonic homogenizer. Fig. 1A shows the photographs of In_2O_3 agglomerates obtained before and after the sonication. Light microscopy revealed that most In_2O_3 agglomerates were dispersed into particles of a few micrometers in size, capable of reaching alveolus in human. The size distribution of In_2O_3 agglomerates showed that the diameters of most particles were distributed from approximately 100 to 500 nm as shown in Fig. 1B. The mean diameter of In_2O_3 agglomerates was 214.5 nm.

Cytotoxicity of In_2O_3

We examined a cytotoxic effect of In_2O_3 on RAW 264.7 cells by trypan blue exclusion assay. Cell viability tended to decrease with increasing In_2O_3 concentrations (Fig. 2). ANOVA plus Tukey's test revealed that In_2O_3 significantly decreased the cell viability at 50 μg/m*l* com-

pared with the control ($p<0.01$, Fig. 2).

8-NitroG formation in In_2O_3 -treated cells

To investigate 8-nitroG formation in RAW 264.7 cells treated with In_2O_3, we performed immunocytochemical analysis. Fig. 3 A shows the formation of 8-nitroG in In_2O_3-treated cells. No or weak staining was observed in non-treated control, and the immunoreactivity of 8-nitroG was increased in In_2O_3-treated cells. 8-NitroG was mainly formed in the nucleus, which was stained with Hoechst 33258. Quantitative image analysis revealed that the staining intensity of 8-nitroG in In_2O_3-treated cells was significantly greater at 20 and 50 μg/m*l* than that in non-treated control ($p<0.05$ and $p<0.01$, respectively, Fig. 3 B). We examined the time course of In_2O_3-induced 8-nitroG formation in RAW 264.7 cells at 20 μg/m*l*, because In_2O_3 induced a clear and significant increase in the staining intensity of 8-nitroG at this concentration. Fig. 4 A shows that In_2O_3 induced 8-nitroG formation at 2 h and its immunoreactivity was further increased at 4 h. Image analysis revealed that In_2O_3 significantly increased 8-nitroG formation at 2 and 4 h compared with the control ($p<0.05$ and $p<0.001$, respectively, Fig. 4B).

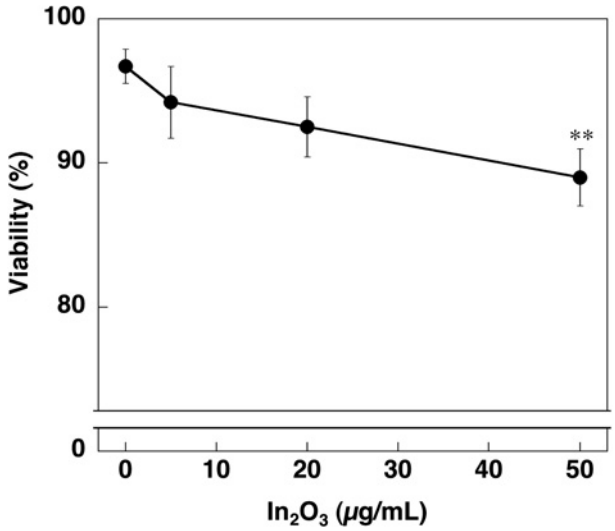

Fig. 2. Cytotoxic effect of In_2O_3 on RAW 264.7 cells. Cells were incubated with indicated concentrations of In_2O_3 for 24 h and cell viability was evaluated by trypan blue exclusion assay. The data were expressed as means ± SD of 3 independent experiments. $^{**}p$ <0.01, compared with the control by ANOVA followed by Tukey's test.

NO release from In_2O_3-treated cells

We measured the levels of NO products, NO_2^- and NO_3^- in culture supernatant of In_2O_3-treated RAW 264.7 cells using nitrate reductase and Griess reagents as shown in Fig. 5. Compared with the control, In_2O_3 significantly increased NO release from the cells at 2 and 4 h ($p<0.01$, Fig. 5). The amount of NO released from In_2O_3-exposed cells was slightly decreased at 4 h compared to that at 2 h (Fig. 5).

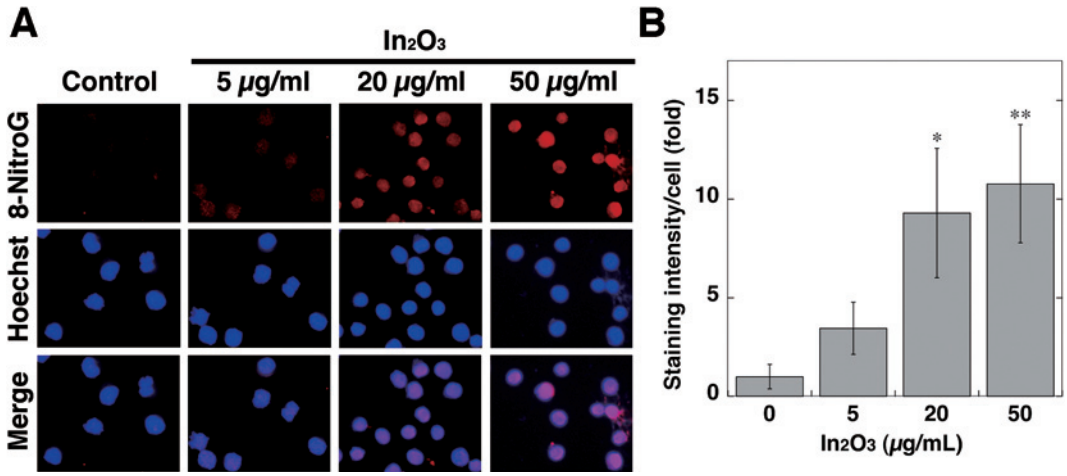

Fig. 3. 8-NitroG formation in In_2O_3-treated cells. (A) Immunofluorescent images of 8-nitroG formation in In_2O_3-treated cells. RAW 264.7 cells were treated with indicated concentrations of In_2O_3 for 4 h at 37°C. 8-NitroG formation was detected by immunocytochemistry as described in Materials and Methods section. The nucleus was stained with Hoechst 33258. Magnification, ×200. (B) Quantitative image analysis of 8-nitroG formation in In_2O_3-treated cells. The staining intensity per cell was quantified with an ImageJ software. The vertical axis shows the fold increase in the staining intensity compared with that of the control, which was set at 1. The data were expressed as means ± SD of 3-4 independent experiments. $^{*}p$ <0.05 and $^{**}p$ <0.01 compared with the control by ANOVA followed by Tukey's test.

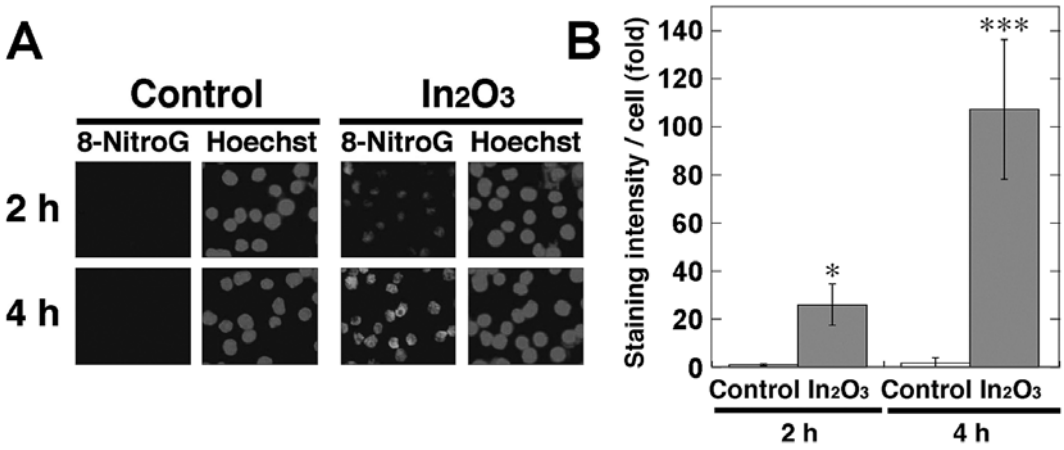

Fig. 4. Time course of 8-nitroG formation in In_2O_3-treated cells. (A) Immunofluorescent images of 8-nitroG formation in In_2O_3-treated cells. RAW 264.7 cells were treated with 20 μg/m*l* of In_2O_3 for indicated durations at 37°C. 8-NitroG formation was detected by immunocytochemistry as described in Materials and Methods section. The nucleus was stained with Hoechst 33258. Magnification, ×200. (B) Quantitative image analysis of 8-nitroG formation in In_2O_3-treated cells. The staining intensity per cell was quantified with an ImageJ software. The vertical axis shows the fold increase in the staining intensity compared with that of the control at 2 h, which was set at 1. The data were expressed as means ± SD of 3-4 independent experiments. *p <0.05 and ***p <0.001 compared with the control by Student's t-test.

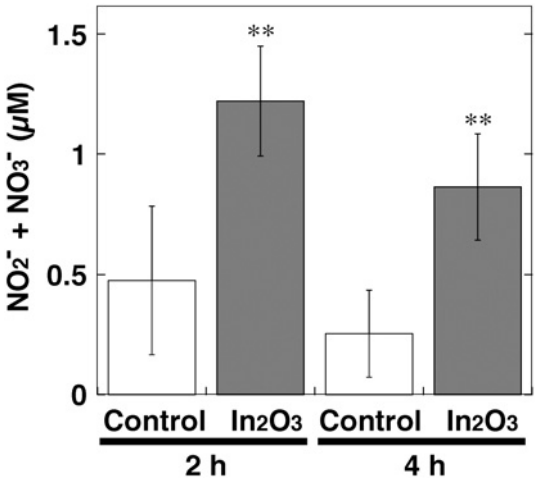

Fig. 5. NO release from In_2O_3-treated cells. RAW 264.7 cells were treated with 20 μg/m*l* of In_2O_3 for indicated durations at 37°C. NO_2^- and NO_3^- levels in the culture supernatant were measured by the Griess method as described in Materials and Methods section. The data were expressed as means ± SD of 4 independent experiments. **p <0.01 compared with control by Student's t-test.

Effects of iNOS and endocytosis inhibitors on In_2O_3-induced 8-nitroG formation

We examined the effects of iNOS and endocytosis inhibitors on In_2O_3-induced 8-nitroG formation in RAW 264.7 cells by immunocytochemistry. In_2O_3 induced clear 8-nitroG formation, and its immunoreactivity was largely suppressed by the treatment with 1400 W (an iNOS inhibitor), MBCD (an inhibitor of caveolae-mediated endocytosis) and MDC (an inhibitor of clathrin-mediated endocytosis) as shown in Fig. 6A. We examined the viability of RAW 264.7 cells treated with In_2O_3 and these inhibitors to confirm that they do not exhibit cytotoxicity. In_2O_3 alone and In_2O_3 plus each inhibitor induced no or slight decrease in the cell viability compared with the control under the conditions used (Fig. 6B), indicating that the reduction in 8-nitroG formation by the inhibitors was not due to their cytotoxic effects. In addition, these inhibitors alone (without In_2O_3) did not show cytotoxic effects (Fig. S1).

Discussion

In this study, we demonstrated that In_2O_3 induced the formation of 8-nitroG, a nitrative DNA lesion, in the nucleus of RAW 264.7 cells. We have previously reported that 8-nitroG was formed at the sites of inflammation-related carcinogenesis in animal models and clinical specimens[16,17,25]. In the lung tissues of asbestos-exposed mice, 8-nitroG was formed in bronchial epithelial cells[26]. The extent of 8-nitroG formation was significantly correlated with asbestos contents in human lung tissues[27]. Multiwalled carbon nanotube and carbon black induced 8-nitroG formation in human lung epithelial cells under occupationally relevant conditions[18-20]. In this study, immunocytochemistry and quantitative image analysis revealed that In_2O_3 significantly increased 8-nitroG formation in RAW 264.7 cells. The concentrations of In_2O_3 in this study appear to be higher than occupationally rele-

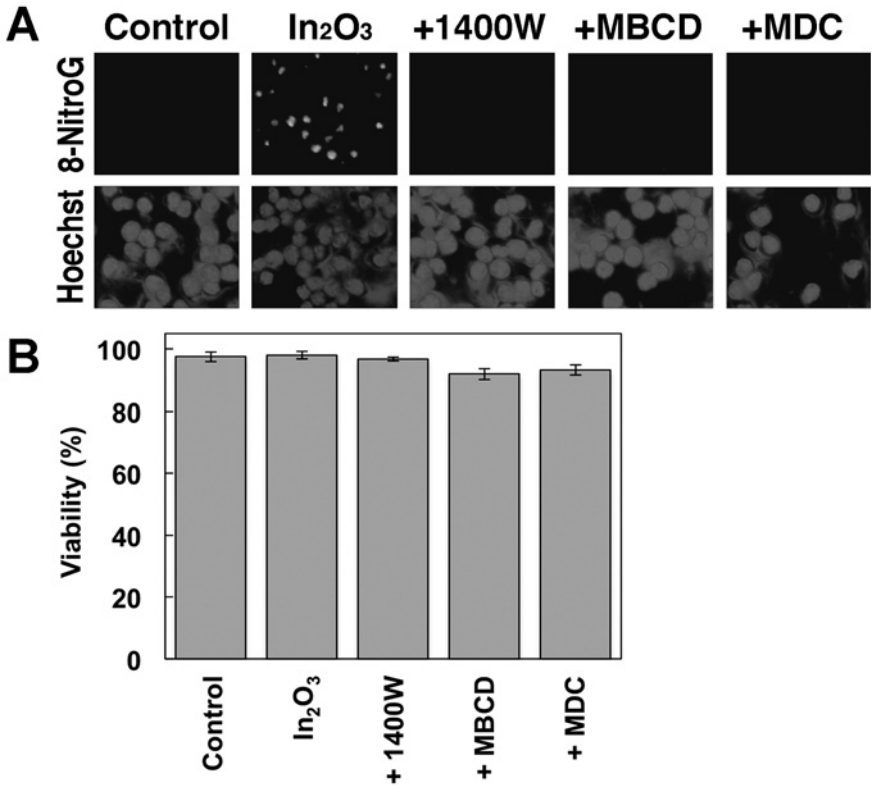

Fig. 6. Effects of iNOS and endocytosis inhibitors on In_2O_3-induced DNA damage and their cytotoxicity. (A) Effects of iNOS and endocytosis inhibitors on In_2O_3-induced 8-nitroG formation. RAW 264.7 cells were treated with 20 μg/m*l* of In_2O_3 for 4 h at 37°C. The cells were co-treated with 1 μM 1400W, 0.5 mM MBCD or 50 μM MDC. 8-NitroG formation was detected by immunocytochemistry as described in Materials and Methods section. The nucleus was stained with Hoechst 33258. Magnification, ×200. (B) Cytotoxicity of In_2O_3 plus inhibitors for iNOS and endocytosis. RAW 264.7 cells were treated with 20 μg/m*l* In_2O_3 plus 1 μM 1400W, 0.5 mM MBCD or 50 μM MDC for 4 h at 37°C. Cell viability was evaluated by trypan blue exclusion assay. The data were expressed as means ± SD of 4 independent experiments.

vant concentrations according to the estimation of alveolar deposition of other types of nanomaterials[19,20], but In_2O_3 caused 8-nitroG formation in a short incubation time of 2 h. Therefore, it is supposed that long-time exposure to indium compounds causes genotoxicity in the respiratory systems even under occupationally relevant conditions. A recent study has demonstrated that indium compounds induced DNA damage in lung epithelial cells, but their concentrations were one or two orders of magnitude greater than those in this study[28]. Therefore, the experimental conditions in this study appear to be more relevant to occupational settings. NO generation was also significantly increased in In_2O_3-treated RAW 264.7 cells. In_2O_3-induced 8-nitroG formation was inhibited by 1400 W, suggesting that 8-nitroG formation is dependent on iNOS expression. The immunoreactivity of 8-nitroG was increased in In_2O_3-exposed cells at 4 h to a greater extent than at 2 h, whereas the amount of NO in the culture supernatant at 4 h was slightly lower than that at 2 h. These results indicate that In_2O_3 initially induced NO generation, which preceded 8-nitroG formation, as demonstrated in previous studies on nanoparticle-induced 8-nitroG formation[19,20]. Nuclear factor-κB (NF-κB) is a transcription factor that regulates expression of various genes involved in inflammatory responses, including iNOS, and ROS and RNS can induce NF-κB activation[29]. These studies raise the possibility that reactive species and NF-κB positively regulate each other and contribute to DNA damage.

8-NitroG is considered to be a potentially mutagenic DNA lesion. The glycoside bond between 8-nitroG and deoxyribose is chemically unstable and thus 8-nitroG can be spontaneously released to form an apurinic site[30]. An apurinic site forms a pair with adenine during DNA replication, leading to G→T transversion[31]. 8-NitroG also forms a pair with adenine and causes a similar type of base substitution[32]. Although recent *in vitro* studies have

demonstrated that indium compounds induce cytotoxicity[33], inflammatory responses[34] and DNA damage[28], this is the first study showing that indium compounds cause NO-dependent DNA damage in cultured cells.

8-NitroG formation induced by In_2O_3 was suppressed by MBCD and MDC, inhibitors of caveolae- and clathrin-mediated endocytosis, respectively. These findings raise a possibility that In_2O_3 particles were initially taken up into cells via endocytosis, resulting in induction of inflammatory responses and DNA damage. The average diameter of In_2O_3 agglomerates was 214.5 nm and the size of most agglomerates was distributed from 100 to 500 nm. Submicron-sized particles are internalized into cells by caveolae- and clathrin-mediated endocytosis[35,36], and inhibitors of clathrin-mediated endocytosis reduced cellular uptake of particles up to 200 nm[35]. We have recently reported that carbon black agglomerates of similar size caused DNA damage in macrophages, which involved clathrin-mediated endocytosis[20]. Therefore, according to the size distribution, In_2O_3-induced DNA damage appears to be, at least in part, accounted for by clathrin-mediated endocytosis. Nanoparticles are considered to induce cell death via the cellular internalization and lysosomal dysfunction[37]. In this study, high dose (50 μg/m*l*) of In_2O_3 significantly decreased the cell viability. These results suggest that In_2O_3 causes cell death in an endocytosis-dependent manner, although the precise mechanism remains to be clarified.

The molecular mechanisms of inflammatory responses induced by particulate matters have been investigated but not well understood. Some studies have demonstrated that fibrous and particulate materials cause inflammatory responses in the respiratory systems via NLRP3 inflammasome in *in vivo* experiments[38]. It has been reported that ITO induced pro-inflammatory responses in a cultured macrophage cell line, which are partially accounted for by inflammasome activation[34]. Recently, we proposed a new mechanism of 8-nitroG formation induced by particulate matters in lung epithelial cell lines, which involves the activation of Toll-like receptor 9 (TLR9) in lysosomes. Particulate matters cause cell injury or necrosis, and the nuclear protein HMGB1 and DNA are released from the cells. Then, the HMGB1-DNA complex interacts with receptor for advanced glycation end-products (RAGE) and is internalized into lysosomes. CpG DNA is recognized by TLR9, leading to NO generation and resulting DNA damage[19]. Recent studies have demonstrated that HMGB1 is internalized into macrophages via endocytosis[39] and that extracellular HMGB1 plus DNA induce TLR9-mediated macrophage activation[40]. Therefore, this pathway may play a substantial role in DNA damage in indium-exposed macrophages in addition to lung epithelial cells. There is a possibility that the reduction in In_2O_3-induced 8-nitroG formation by endocytosis inhibitors is partially accounted for by suppression of cellular uptake of the HMGB1-DNA-RAGE complex.

In conclusion, we have demonstrated that In_2O_3 induced nitrative DNA damage in cultured cells, and this event involves endocytosis and iNOS-dependent NO generation. NO released from indium-exposed inflammatory cells, including macrophages, may induce DNA damage not only in these cells but also in adjacent lung epithelial cells, which may contribute to indium-induced carcinogenesis.

Acknowledgments : This work was supported by Grants-in-Aid for Scientific Research from the Ministry of Education, Science, Sports and Culture of Japan (Grant numbers 25670313 and 15H04784).

Conflict of interest: None declared.

References

1) Homma T, Ueno T, Sekizawa K, Tanaka A, Hirata M. Interstitial pneumonia developed in a worker dealing with particles containing indium-tin oxide. J Occup Health 2003; 45: 137-139.
2) Chonan T, Taguchi O, Omae K. Interstitial pulmonary disorders in indium-processing workers. Eur Respir J 2007; 29: 317-324.
3) Choi S, Won YL, Kim D, et al. Interstitial lung disorders in the indium workers of Korea: an update study for the relationship with biological exposure indices. Am J Ind Med 2015; 58: 61-68.
4) Cummings KJ, Donat WE, Ettensohn DB, Roggli VL, Ingram P, Kreiss K. Pulmonary alveolar proteinosis in workers at an indium processing facility. Am J Respir Crit Care Med 2010; 181: 458-464.
5) Xiao YL, Cai HR, Wang YH, Meng FQ, Zhang DP. Pulmonary alveolar proteinosis in an indium-processing worker. Chin Med J (Engl) 2010; 123: 1347-1350.
6) Nakano M, Omae K, Uchida K, et al. Five-year cohort study: emphysematous progression of indium-exposed workers. Chest 2014; 146: 1166-1175.
7) Nagano K, Nishizawa T, Umeda Y, et al. Inhalation carcinogenicity and chronic toxicity of indium-tin oxide in rats and mice. J Occup Health 2011; 53: 175-187.
8) Guha N, Loomis D, Guyton KZ, et al. Carcinogenicity of welding, molybdenum trioxide, and indium tin oxide. Lancet Oncol 2017; 18: 581-582.
9) IARC. IARC Monographs on the Evaluation of Carcinogic Risks to Humans, vol. 118, Welding, Welding Fumes, and Some Related Chemicals. in press.
10) IARC. Indium Phosphide. In: IARC Monographs on the Evaluation of Carcinogic Risks to Humans, vol. 86, Cobalt in Hard Metals and Cobalt Sulfate, Gallium Arsenide, Indium Phosphide and Vanadium Pentoxide. 2006. p. 197-224.
11) Balkwill F, Mantovani A. Inflammation and cancer: back to Virchow? Lancet 2001; 357: 539-545.
12) Coussens LM, Werb Z. Inflammation and cancer. Nature

2002; 420: 860-867.
13) Hussain SP, Hofseth LJ, Harris CC. Radical causes of cancer. Nat Rev Cancer 2003; 3: 276-285.
14) Ohshima H, Tatemichi M, Sawa T. Chemical basis of inflammation-induced carcinogenesis. Arch Biochem Biophys 2003; 417: 3-11.
15) Yermilov V, Rubio J, Becchi M, Friesen MD, Pignatelli B, Ohshima H. Formation of 8-nitroguanine by the reaction of guanine with peroxynitrite *in vitro*. Carcinogenesis 1995; 16: 2045-2050.
16) Kawanishi S, Hiraku Y, Pinlaor S, Ma N. Oxidative and nitrative DNA damage in animals and patients with inflammatory diseases in relation to inflammation-related carcinogenesis. Biol Chem 2006; 387: 365-372.
17) Hiraku Y. Formation of 8-nitroguanine, a nitrative DNA lesion, in inflammation-related carcinogenesis and its significance. Environ Health Prev Med 2010; 15: 63-72.
18) Guo F, Ma N, Horibe Y, Kawanishi S, Murata M, Hiraku Y. Nitrative DNA damage induced by multi-walled carbon nanotube via endocytosis in human lung epithelial cells. Toxicol Appl Pharmacol 2012; 260: 183-192.
19) Hiraku Y, Guo F, Ma N, et al. Multi-walled carbon nanotube induces nitrative DNA damage in human lung epithelial cells via HMGB1-RAGE interaction and Toll-like receptor 9 activation. Part Fibre Toxicol 2016; 13: 16.
20) Hiraku Y, Nishikawa Y, Ma N, et al. Nitrative DNA damage induced by carbon-black nanoparticles in macrophages and lung epithelial cells. Mutat Res 2017; 818: 7-16.
21) Valavanidis A, Vlachogianni T, Fiotakis K, Loridas S. Pulmonary oxidative stress, inflammation and cancer: respirable particulate matter, fibrous dusts and ozone as major causes of lung carcinogenesis through reactive oxygen species mechanisms. Int J Environ Res Public Health 2013; 10: 3886-3907.
22) Schmall A, Al-Tamari HM, Herold S, et al. Macrophage and cancer cell cross-talk via CCR2 and CX3CR1 is a fundamental mechanism driving lung cancer. Am J Respir Crit Care Med 2015; 191: 437-447.
23) Pinlaor S, Hiraku Y, Ma N, et al. Mechanism of NO-mediated oxidative and nitrative DNA damage in hamsters infected with *Opisthorchis viverrini*: a model of inflammation-mediated carcinogenesis. Nitric Oxide 2004; 11: 175-183.
24) Hiraku Y, Kawanishi S. Immunohistochemical analysis of 8-nitroguanine, a nitrative DNA lesion, in relation to inflammation-associated carcinogenesis. In: Walker J, editor. Methods in Molecular Biology. vol. 512. New York: Springer; 2009. p. 3-13.
25) Kawanishi S, Hiraku Y. Oxidative and nitrative DNA damage as biomarker for carcinogenesis with special reference to inflammation. Antioxid Redox Signal 2006; 8: 1047-1058.
26) Hiraku Y, Kawanishi S, Ichinose T, Murata M. The role of iNOS-mediated DNA damage in infection- and asbestos-induced carcinogenesis. Ann NY Acad Sci 2010; 1203: 15-22.
27) Hiraku Y, Sakai K, Shibata E, et al. Formation of the nitrative DNA lesion 8-nitroguanine is associated with asbestos contents in human lung tissues: a pilot study. J Occup Health 2014; 56: 186-196.
28) Tabei Y, Sonoda A, Nakajima Y, et al. Intracellular accumulation of indium ions released from nanoparticles induces oxidative stress, proinflammatory response and DNA damage. J Biochem 2016; 159: 225-237.
29) Blaser H, Dostert C, Mak TW, Brenner D. TNF and ROS crosstalk in inflammation. Trends Cell Biol 2016; 26: 249-261.
30) Yermilov V, Rubio J, Ohshima H. Formation of 8-nitroguanine in DNA treated with peroxynitrite in vitro and its rapid removal from DNA by depurination. FEBS Lett 1995; 376: 207-210.
31) Loeb LA, Preston BD. Mutagenesis by apurinic/apyrimidinic sites. Annu Rev Genet 1986; 20: 201-230.
32) Suzuki N, Yasui M, Geacintov NE, Shafirovich V, Shibutani S. Miscoding events during DNA synthesis past the nitration-damaged base 8-nitroguanine. Biochemistry 2005; 44: 9238-9245.
33) Gwinn WM, Qu W, Bousquet RW, et al. Macrophage solubilization and cytotoxicity of indium-containing particles as *in vitro* correlates to pulmonary toxicity *in vivo*. Toxicol Sci 2015; 144: 17-26.
34) Badding MA, Schwegler-Berry D, Park JH, Fix NR, Cummings KJ, Leonard SS. Sintered indium-tin oxide particles induce pro-inflammatory responses *in vitro*, in part through inflammasome activation. PLoS One 2015; 10: e0124368.
35) Rejman J, Oberle V, Zuhorn IS, Hoekstra D. Size-dependent internalization of particles via the pathways of clathrin- and caveolae-mediated endocytosis. Biochem J 2004; 377: 159-169.
36) Gratton SE, Ropp PA, Pohlhaus PD, et al. The effect of particle design on cellular internalization pathways. Proc Natl Acad Sci USA 2008; 105: 11613-11618.
37) Stern ST, Adiseshaiah PP, Crist RM. Autophagy and lysosomal dysfunction as emerging mechanisms of nanomaterial toxicity. Part Fibre Toxicol 2012; 9: 20.
38) Jessop F, Holian A. Extracellular HMGB1 regulates multi-walled carbon nanotube-induced inflammation *in vivo*. Nanotoxicology 2015; 9: 365-372.
39) Xu J, Jiang Y, Wang J, et al. Macrophage endocytosis of high-mobility group box 1 triggers pyroptosis. Cell Death Differ 2014; 21: 1229-1239.
40) Li X, Yue Y, Zhu Y, Xiong S. Extracellular, but not intracellular HMGB1, facilitates self-DNA induced macrophage activation via promoting DNA accumulation in endosomes and contributes to the pathogenesis of lupus nephritis. Mol Immunol 2015; 65: 177-188.